Observation of Ultrafast Intersystem Crossing in Thymine by Extreme Ultraviolet Time-resolved Photoelectron Spectroscopy

Thomas J. A. Wolf[†,*], *Robert M. Parrish*[‡,#], *Rolf H. Myhre*[§], *Todd J. Martínez*[‡,#], *Henrik Koch*[∥], *Markus Gühr*[†,⊥,*]

[†]Stanford PULSE Institute, SLAC National Accelerator Laboratory, Menlo Park, USA.

[‡]Department of Chemistry, Stanford University, Stanford, USA. [§]Department of Chemistry, Norwegian University of Science and Technology, NO-7491 Trondheim, Norway.

[∥]Scuola Normale Superiore, Piazza dei Cavalieri, 7, 56126 Pisa PI, Italy.

[⊥]Institut für Physik und Astronomie, Universität Potsdam, Potsdam, Germany.

KEYWORDS Nucleobases, Photoprotection, Excited state dynamics, Intersystem crossing

ABSTRACT We studied the photoinduced ultrafast relaxation dynamics of the nucleobase thymine using gas-phase time-resolved photoelectron spectroscopy. By employing extreme ultraviolet pulses from high harmonic generation for photoionization, we substantially extend our spectral observation window with respect to previous studies. This enables us to follow relaxation of excited state population all the way to low-lying electronic states including the

ground state. In thymine, we observe relaxation from the optically bright $^1\pi\pi^*$ state of thymine to a dark $^1n\pi^*$ state within (80 ± 30) fs. The $^1n\pi^*$ state relaxes further within (3.5 ± 0.3) ps to a low-lying electronic state. By comparison with quantum chemical simulations, we can unambiguously assign its spectroscopic signature to the $^3\pi\pi^*$ state. Hence, our study draws a comprehensive picture of the relaxation mechanism of thymine including ultrafast intersystem crossing to the triplet manifold.

Introduction

The ultrafast excited state dynamics of the nucleobases, the DNA and RNA building blocks, have attracted a lot of research interest. With absorption cross-sections of 10s of Mbarns, they are among the strongest UV chromophores in nature. However, lesions in DNA triggered by the substantial absorbed photon energies are a comparably rare event,[1] which might be the reason for the evolutionary selection of the DNA molecules in early earth history. From femtosecond pump-probe studies, it is known that the reason for the low photoreactivity is an ultrafast photoprotection mechanism involving non-Born-Oppenheimer relaxation dynamics through conical intersections. Despite a high number of experimental and theoretical investigations (see reviews[2–4] and refs. cited therein), the details of the photoprotection mechanism, specifically in the pyrimidine nucleobases cytosine, thymine, and uracil, are still heavily under debate. These details are most thoroughly investigated in isolated molecules in the gas phase, since the molecular response is not obscured by contributions from the environment and the results can be compared to high-level quantum chemical simulations.[5–7]

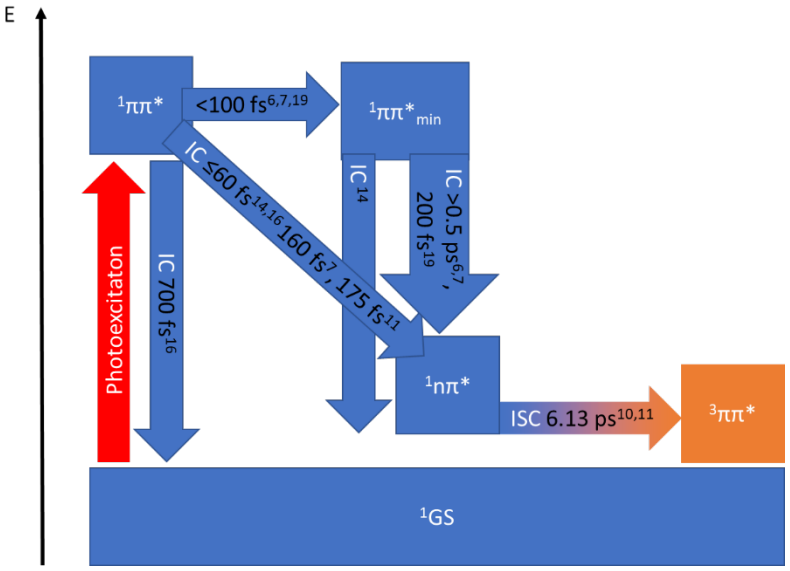

The focus of our present investigation is thymine, which is distinct from the other nucleobases in two aspects: It has been observed to show relaxed states in the gas phase with lifetimes beyond the ultrafast regime[8–11] and it is the nucleobase responsible for the main photoinduced mutagenic product in DNA.[12] Thymine can be photoexcited at 267 nm to a state with ππ* electronic character. Additionally, it exhibits another, dark excited state with nπ* character. Several relaxation pathways have been proposed in experimental and theoretical studies, which are summarized in Fig. 1. A number of studies found evidence for trapping of population in a $^1\pi\pi^*$ state minimum for several hundred fs or even ps, followed by relaxation to either the $^1n\pi^*$ state[6,7,12,13] or the ground state.[14] Others find rapid relaxation within ~100 fs to the $^1n\pi^*$ state[7,11,15] or the ground state.[16] In our own recent study employing a combination of time-

resolved near-edge x-ray absorption fine structure (TR-NEXAFS) spectroscopy and coupled cluster calculations, we could unambiguously prove that at least a substantial part of the $^1\pi\pi^*$ state population relaxes within 60 fs through a conical intersection to the $^1n\pi^*$ state.[17] Our TR-NEXAFS study, however, could not exclude part of the population being trapped in the $^1\pi\pi^*$ state and relaxing directly to the ground state. The existence of such a competing relaxation channel is supported by observations of considerably larger $^1\pi\pi^*$ state lifetimes than in TR-NEXAFS by methods like time-resolved photoelectron spectroscopy (TRPES) and Auger electron spectroscopy, which are directly sensitive to the $^1\pi\pi^*$ state population.[11,18,19] It can, however, not be excluded that those lifetimes are limited by the time resolution of the respective experimental studies. Fast signal decays with time constants of on the order of 100 fs have also been observed in two time-resolved multiphoton-ionization studies.[8,20] In one of these studies, it was, however, interpreted as an artifact caused by resonance enhancement of the multiphoton ionization process.[8,21,22]

The observation of features with lifetimes on the ns time scale after photoexcitation of thymine has been attributed to a triplet state with $\pi\pi^*$ character[10,11] (see Fig. 1). It has been argued that triplet states play an important role in DNA damage mechanisms due to their high lifetime.[23] Theoretical studies found high spin-orbit coupling strengths in the area of the $^1n\pi^*$ minimum.[7,24] This suggests an intersystem crossing (ISC) channel from the $^1n\pi^*$ state to the $^3\pi\pi^*$ state. While ISC was for long believed not to proceed on (sub) ps time scales, more recent studies prove it to be a rather common effect on ultrafast time scales and in organic molecules exhibiting excited states with $n\pi^*$ character.[7,25-27] In fact, ultrafast intersystem crossing was predicted for thymine by nonadiabatic dynamical simulations.[7] The triplet state can be expected to exhibit a characteristic TRPES signature. However, its ionization potential (IP) is comparably high (8 eV, see below).

The signature, therefore, could not have been observed in a one photon ionization process by existing TRPES studies employing probe photon energies ≤ 6.2 eV in the UV.[11,18]

In our present TRPES study we, therefore, employ probe photon energies in the extreme ultraviolet (EUV) beyond the IP of thymine. Together with ab initio molecular dynamics simulations, they enable us to unambiguously prove population of the $^3\pi\pi^*$ state on the ps time scale. Our <100 fs instrument response function, furthermore, enables us to revisit the question of different depopulation channels for the $\pi\pi^*$ state with an unprecedented temporal resolution.

Experimental and Theoretical Methods

Experimental

The EUV-TRPES spectra were recorded in an apparatus described in detail elsewhere.[28,29] In short, we used a commercial femtosecond laser system providing pulses with an energy of 7 mJ and 30 fs duration and 800 nm central wavelength. A minor fraction of the pulse energy was frequency tripled and reflectively focused into the interaction region of a magnetic bottle photoelectron spectrometer to excite thymine at 267 nm. The majority of the pulse energy was focused by a lens (f=1670 mm) into a 1 mm long high harmonic gas cell. Xenon was used for high harmonic generation at pressures in the single torr regime. The majority of the seed laser light copropagating with the high harmonics was removed by reflecting off a silicon wafer under an angle of incidence of 81°. An indium filter (150 nm thickness) was used to remove the remaining seed laser light and to suppress all but the 9th harmonic of the seed laser at 14 eV. The 9th harmonic was subsequently focused into the interaction region and quasi-collinearly overlapped with the focus of the third harmonic excitation pulse. Care was taken to overfill the focus of the 9th harmonic (100 μm) with the pump focus (140 μm). Thymine was evaporated at

160 °C into the interaction region of the magnetic bottle photoelectron spectrometer using an in-vacuum oven,[30] leading to a sample density on the order of 10^{12} cm^{-3}. Time-dependent photoelectron spectra were recorded by alternatingly collecting photoelectron spectra at a negative reference time delay and the target time delay. The spectrometer flight tube was biased with a low negative voltage to prevent photoelectrons created by the pump pulse from detection. The instrument response function was independently determined by pump-probe two-photon ionization of argon to be 90 fs.

Theoretical:

Stationary points in the electronic ground state and singlet excited states were optimized on coupled cluster level. The geometries and the details of the electronic structure method can be found in Ref.[17] and its supplement. The minimum geometry of the lowest triplet state was optimized at the CCSD level. Valence ionization potentials at those geometries were calculated on CCSD/aug-cc-pVDZ level. Ionization cross-sections were evaluated based on Dyson orbitals using EOM-CCSD. We used the QCHEM and Dalton programs for these calculations.[31,32]

For simulating the long time-limit photoelectron spectra of the "hot" singlet ground state and ππ* triplet state, a procedure was developed to approximate sampling molecular geometries from the long-time limit of the photodynamics without requiring explicit simulation of the non-adiabatic dynamics through methods such as AIMS. AIMD computations for the singlet ground state and ππ* triplet state were performed in TeraChem and started from the respective minimum geometries at the B3LYP/6-31G** level.[33–42] The excess vibrational energy of the pump photon was initially randomly distributed as kinetic energy (momenta) drawn from a Maxwellian distribution. In the case of the hot ground state spectrum, the excess vibrational energy was selected to be the TDA-TD-DFT B3LYP/6-31G** S_0-S_1 vertical excitation energy of 4.77 eV (in

close agreement with the experimental pump energy of 4.65 eV).[43] In the case of the triplet state, the excess vibrational energy was selected to be the difference between TDA-TD-DFT B3LYP/6-31G** S_0-S_1 vertical excitation energy of 4.77 eV and the UB3LYP/6-31G** S_0-T_1 excitation energy of 2.92 eV, for a total excess kinetic energy of 1.85 eV. In each case, the total vibrational energy was then computed as the excess vibrational energy plus 3.27 eV of vibrational energy representing the ZPVE and average thermal contributions for a 300 K harmonic Wigner distribution at B3LYP/6-31G** on S_0. The total vibrational energy was then randomly distributed with a Maxwellian distribution. From these initial conditions, NVE AIMD simulations were propagated adiabatically for the singlet and triplet states for 8 ps to redistribute the excess kinetic energy to the anharmonic modes of the full molecular system – 3x separate trajectories were run for singlet and for triplet. 50 random geometries were sampled from the last 4 ps of the AIMD trajectory to avoid any bias from the Maxwellian initial conditions. Overall, this procedure generates molecular snapshots which are energetically consistent with long-time-limit AIMS simulations which have decayed from S_1 back to S_0 or T_1. For each of those 50 geometries, IPs and cross-sections were evaluated using EOM-CCSD. The resulting stick spectra were broadened with Lorentzian line shapes.

Results

In Fig. 2, we show the TRPES spectra of thymine in a photoelectron kinetic energy (PEKE) region between 6.3 and 9.5 eV. Our experimental dataset extends farther to lower PEKEs. However, the signatures below 6.3 eV are more difficult to interpret, since they arise from ionization into higher-lying ionic continua. Furthermore, additional contributions from the ground state PE spectrum below 5 eV complicate their interpretation. The observable features in

Fig. 2 agree very well with earlier published studies.[11,18] However, our PEKE window (3.2 eV) is considerably larger than in those studies due to our considerably higher probe photon energies.

Based on their appearance times and decay time scales, we categorize the observable signatures into three regions (see Fig. 2). The fastest change in the spectra – apart from turn on of transient signal at time zero – takes place in the regime between 8.2 and 9.5 eV labeled as Region I. It contains a broad signature at relatively high PEKEs, which decays with a lifetime < 100 fs. In the region between 7 and 8 eV (Region II), a strong signature appears slightly delayed with respect to Region I and considerably shifted to lower PEKEs (see Supporting Figure 1 for a comparison of the time-dependent intensities of Region I and II). It experiences a spectral shift towards a lower PEKE region (6.3 - 7.5 eV, Region III) within <10 ps. The resulting signature is stable in the investigated time window of 40 ps. The relative timing of the signatures in

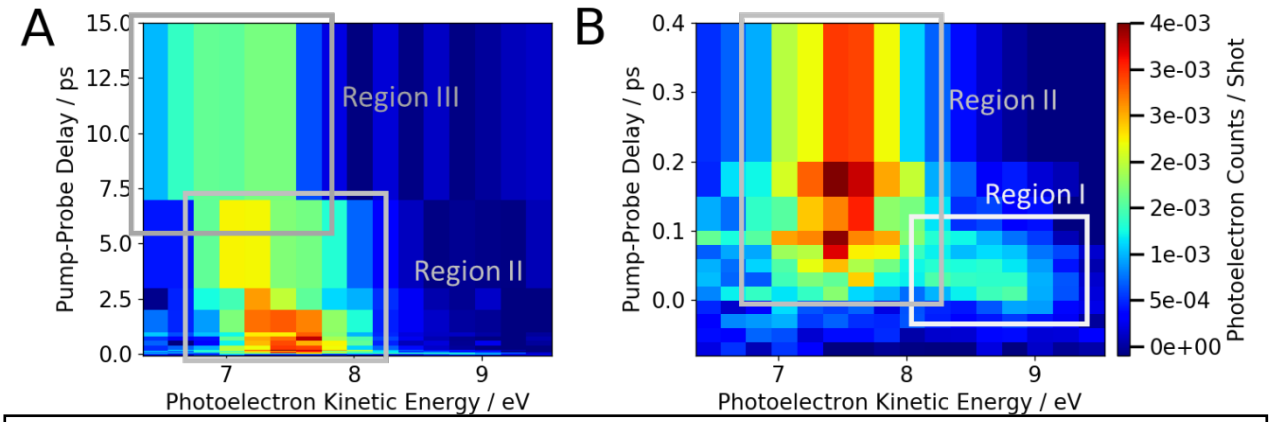

regions I-III suggests that they are due to consecutive relaxation processes. We, therefore, rationalize the signal with a three-exponential global fit[18] of the form

$$S(E,t) = g(t) \otimes \sum_{i=1}^{3} A_i(E) \cdot e^{-\frac{t}{\tau_i}}$$

where S(E,t) is the fitted time and PEKE-dependent spectrum, $A_i(E)$ the so-called decay-associated difference spectra (DADS) associated with exponential time constants τ_i, and g(t) a Gaussian instrument response function.

The DADS resulting from the global fit are shown in Fig. 3. They exhibit a clear connection

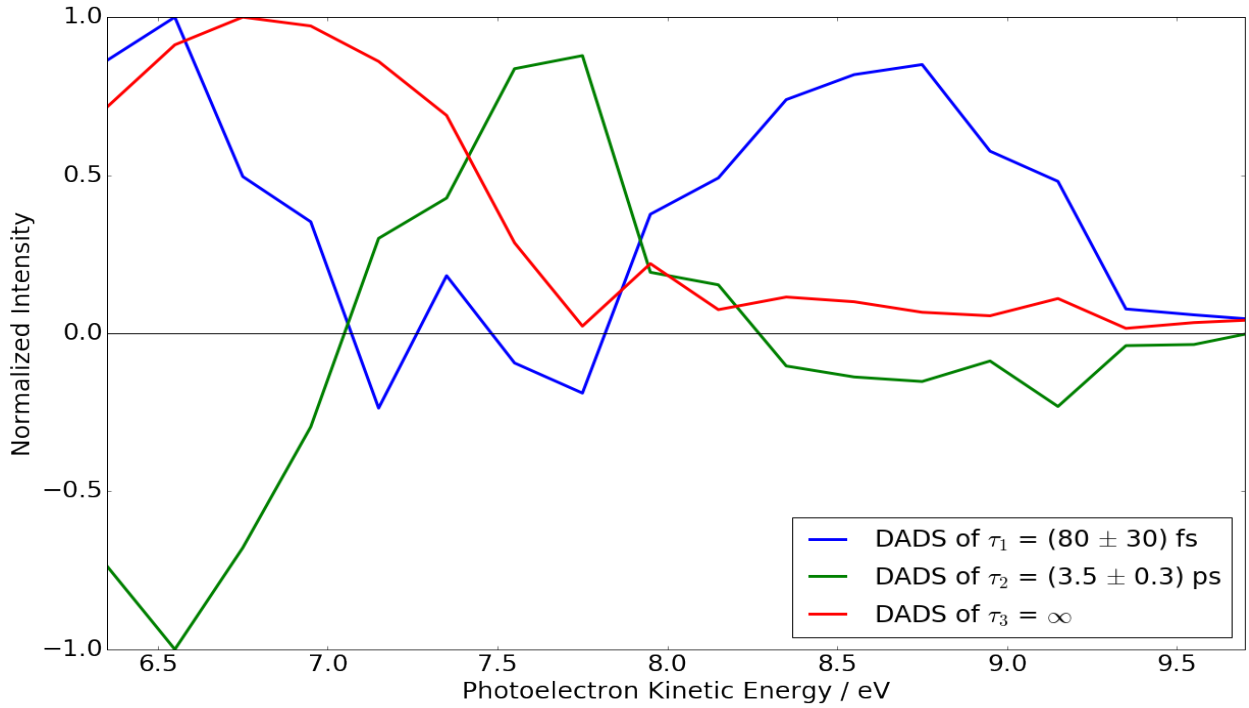

between the three time constants and the spectral signatures in region I-III. The DADS connected to τ_1 = (80 ± 30) fs shows a positive signature in region I and some negative contribution in region II. Thus, τ_1 is both connected to an exponential decay of intensity in region I and an intensity increase in region II. The fact that the negative contribution in region II is not very pronounced is due to substantial difference in intensities in region I and II and a tilt in the region I signatures (see below), which induce small artifacts to the DADS. The timing of the region I and II signals is, however, obvious in Supporting Figure 1. The DADS exhibits an additional positive signature at kinetic energies < 7 eV, which is most likely due to a higher-lying ionic state. Similar considerations on the DADS connected to the time constant τ_2 = (3.5 ± 0.3) ps prove that it simultaneously describes an exponential decay of intensity in region II and an increase of intensity in region III. Since the signal in region III does not decay on the investigated timescale, the value of its time constant τ_3 cannot be accurately described. We will in the following discuss the signal evolution in the three regions separately.

Discussion

Region I

Region I contains a broad photoelectron (PE) signature which exhibits a slight tilt towards later delays and lower PEKE's. This effect is more obvious, when each spectral slice of the TRPES spectrum is normalized to its temporal maximum (see Supporting Fig. 2). Immediately after photoexcitation, thymine can be expected to relax out of the Franck-Condon region of the $^1\pi\pi^*$ state. The shape of the signature fits very well to this expectation: The high-energy cutoff of the PE signature at 9.3 eV, which is appearing first, agrees well with the difference between the combined pump and probe photon energies (4.7 eV and 14.0 eV) and the ground state IP (9.2 eV[44]). Due to redistribution of potential energy into kinetic energy in the Franck-Condon active

nuclear degrees of freedom and different shapes of excited state and cationic state potentials, the $^1\pi\pi^*$ IP can be expected to increase along the relaxation coordinate. This is also reflected in our calculations and the underlying reason for the tilt of the signature towards lower PEKEs at later delays.

Similar tilts at time zero are frequently observed in fs TRPES spectra.[45,46] While our global fit does not account for the tilt, it can be described analytically by employing a step ladder model as detailed in Ref.[46]. Since the tilt is small with respect to the temporal width of the band, we refrain from expanding our global fit with a stepladder model.

The broad feature in region I was observed in the earlier TRPES studies on thymine.[11,18] As already mentioned in the introduction, it was connected with a considerably larger time constant (175 fs vs. (80 ± 30) fs in the present case),[11] which, furthermore, agrees well with a time constant assigned to $^1\pi\pi^*$ state depopulation in a time-resolved Auger electron spectroscopy study.[19] Our smaller time constant suggests that the observations in the earlier studies are dominated by their time-resolution (200 fs vs. 90 fs in the present case).[11] This is further supported by the fact that the tilt we observe in region I has not been reported before. Our findings agree within the error bars very well with the observed delay in onset of the $n\pi^*$ state signature ((60± 30) fs) in our TR-NEXAFS study.[17] Thus, we do not find any evidence for a second channel trapping a fraction of population in the $^1\pi\pi^*$ state. Similar time constants have also been observed in time-resolved multiphoton photoion spectroscopy experiments of thymine.[8,20]

Region II

According to our global fit, the signature in region I decays within (80 ± 30) fs and simultaneously gives rise to a more intense signature in region II, which is stable on the ps timescale. The process is accompanied by a considerable increase in IP by 1.7 eV, which is most

likely due to a sudden change in electronic character during internal conversion between the $^1\pi\pi^*$ state and the $^1n\pi^*$ state.[47] The different electronic characters correspond to different Koopmans-correlated ionic continua with π^{-1} and n^{-1} character.[48] The attribution to $^1\pi\pi^*/^1n\pi^*$ internal conversion, again, agrees very well with the findings of our recent TR-NEXAFS study.[17] Furthermore, our investigations of the $^1\pi\pi^*$ PES on coupled cluster level[17] could not confirm the $^1\pi\pi^*$ minima and barriers obtained in earlier studies on different multi-reference levels.[6,7,49,50] Instead, we could identify a $^1\pi\pi^*/^1n\pi^*$ intersection seam close to the Franck-Condon region. The occurrence of the $^1\pi\pi^*$ minimum in studies employing multi-reference methods is sensitively dependent on the choice of the active space, the treatment of dynamic electron correlation, and the employed basis set. Coupled cluster methods, on the other hand, can fail to describe excited state potentials correctly, e.g. close to conical intersections with the ground state. In the case of the $^1\pi\pi^*$ minimum, however, our coupled cluster approach can be expected to yield a qualitatively correct description of the excited state potential. Other than in the $^1\pi\pi^*$ state, we found a shallow double-minimum in the $^1n\pi^*$ state connected by a saddle point with C_s symmetry, which might be able to trap the population for several picoseconds.

However, it is not trivial to confirm the assignment of the feature in region II to this minimum. We calculate the IP of the $^1n\pi^*$ minimum to the n^{-1} continuum to be 5.65 eV (CCSD/aDZ, see the methods section in the supporting information). This corresponds to a predicted PEKE of 8.3 eV, which is considerably higher than the experimentally observed peak maximum of 7.3 eV in region II and, therefore, underestimates the IP by 1 eV. The calculations, on the other hand, also exclude the possibility of the feature resulting from trapped $^1\pi\pi^*$ population, since any calculated $^1\pi\pi^*$ IPs are below the $^1n\pi^*$ state minimum IP leading to an even larger underestimation. Thus, the TRPES signature of the population in the $^1n\pi^*$ state is not well described by the vertical IP at

the minimum. There are two main reasons for that: According to our calculations, relaxation from the $^1\pi\pi^*$ Franck-Condon region to the $^1n\pi^*$ minimum redistributes 0.3 eV of the absorbed photon energy into vibrational degrees of freedom. Furthermore, as described above, the $^1n\pi^*$ minimum is shallow. The nuclear wavepacket can, therefore, be expected to be broad. To assess, if the IP exhibits strong modulations around the $^1n\pi^*$ minimum, we scanned it along the lowest vibrational mode[17] (see Supporting Fig. 3). Already in this mode, we find an increase in the IP by 0.4 eV whereas the potential energy in the $n\pi^*$ state only increases by 0.03 eV. The fact that the $n\pi^*$ minimum exhibits several low-frequency modes[17] convinces us that the broadness of the wavepacket can account for the observed disagreement between calculated IP and observed TRPES signature. A more reliable test would be comparison of the TRPES bands to signatures based on excited state wavepacket simulations, giving a more complete picture of the directions, in which the IP needs to be scanned.[46,51] The available standard electronic structure methods for such dynamics, however, predict a qualitatively different relaxation process, wavepacket trapping in a $^1\pi\pi^*$ state minimum. Thus, they cannot be used to calculate photoelectron features connected to a process that we identified by independent means: the sub-100 fs $^1\pi\pi^*/^1n\pi^*$ internal conversion.

Region III

The signature in region III is considerably shifted to lower PEKEs with respect to region II i.e. arises from population of a state with a considerably higher IP than the $^1n\pi^*$ state. Therefore, its band has not been observed in earlier studies due to insufficient probe photon energies. Its intensity maximum appears at 6.7 eV, 2.2 eV above the first photoelectron band of the cold ground state. Its lifetime outside our investigated time window permits essentially two possibilities for the nature of this state, the singlet ground state and the lowest triplet state with

ππ* character. A third possibility, photofragmentation, can be excluded based on a previous study.[52] Both relaxation from the ^{1}nπ* state to the ground state[7] and relaxation via ISC to the lowest-lying triplet state with ππ* character permitted by a specifically large spin-orbit coupling

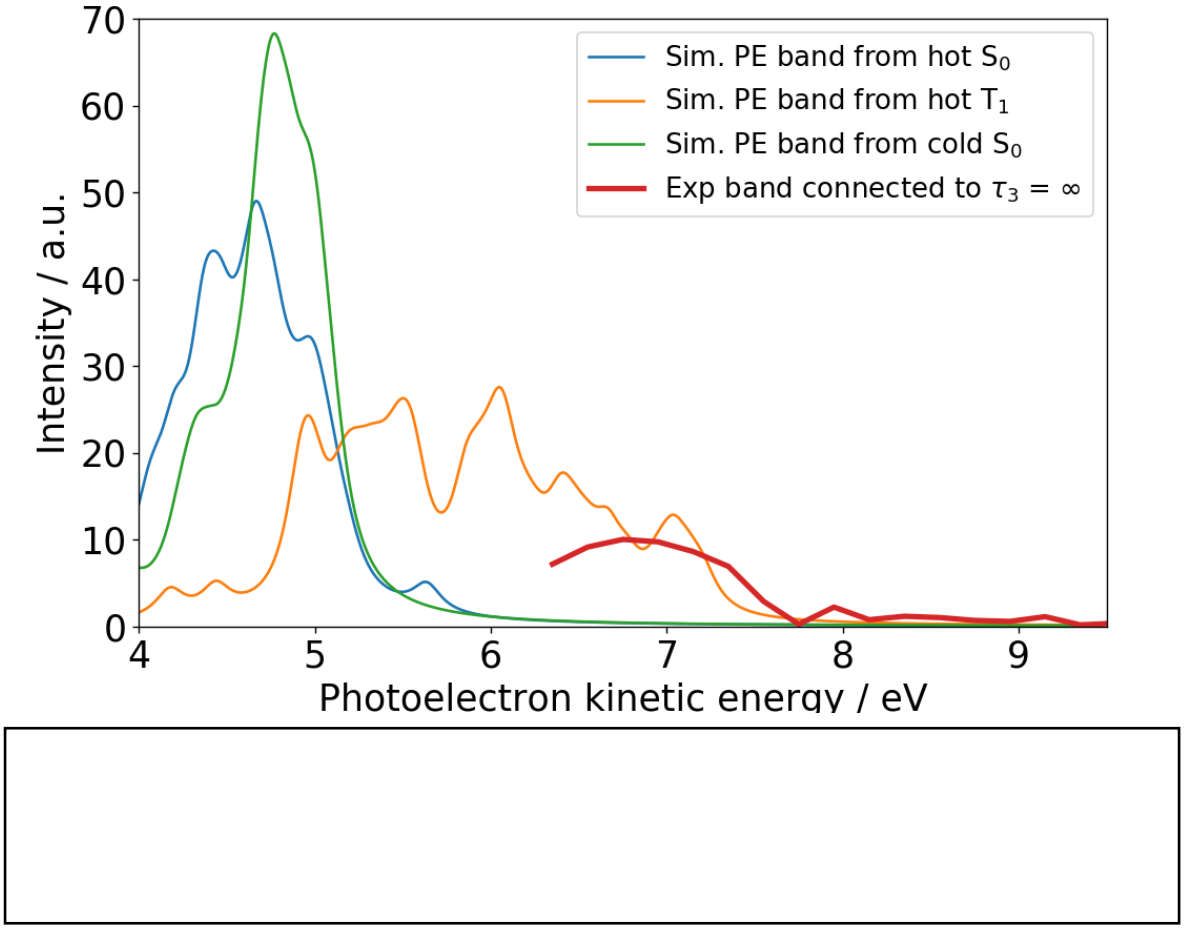

at the nπ* minimum have been proposed in experimental and theoretical studies.[7,11,24]

The high amount of energy redistributed into vibrational motion after relaxation to either the singlet ground state or the ππ* triplet state further increases the difficulties already encountered in assigning the feature in region II to the ^{1}nπ* state. Hence, it cannot be excluded by a single calculated IP at the minimum geometry that vibrational excitation could lead to a shift of the ground state photoelectron band by 2.2 eV. However, the states exhibit a significantly higher

lifetime than the nπ* state. The higher lifetime permits the molecules to achieve a microcanonical distribution of the vibrational energy among the nuclear degrees of freedom. Additionally, both states can be reliably accessed with comparably cheap theoretical methods. We, therefore, simulated the spectra from the singlet ground state and the $^3\pi\pi^*$ state based on AIMD simulations (see methods). The resulting spectra are shown together with the experimental signature in Fig. 4. The comparison shows clearly, that only the simulated spectrum of the hot $^3\pi\pi^*$ state agrees with the experimental signature. This finding represents the first unambiguous proof that thymine undergoes ISC to the triplet manifold within (3.5 ± 0.3) ps after photoexcitation.

The value of our ISC time constant is considerably smaller than corresponding time constants reported before in TRPES and time-resolved photoion spectroscopy studies.[8,11,18,20] In the case of the TRPES studies,[11,18] this can be explained by the lower employed probe photon energy. An accurate fit result of the ISC time constant requires the ability to reliably detect both the $^1n\pi^*$ state and the $^3\pi\pi^*$ state. In both studies, the long-lived signal can come only from the high kinetic energy edge of the triplet signature. This makes the time constant highly sensitive to changes in the width of this signature. Additionally, it is known that multiphoton ionization can induce artifacts due to resonant intermediate states.[21] In contrast to our present results, we observed a biexponential decay of the nπ* signature with time constants of (1.9 ± 01) ps and (10.5 ±0.2) ps in our earlier TR-NEXAFS study.[17] The reasons for this disagreement are not immediately obvious and require further investigation. We speculate that ISC might proceed via an additional geometry minimum of the $^1n\pi^*$ state with a different NEXAFS cross-section.

Conclusion

In conclusion, our study reveals a comprehensive picture of the relaxation mechanism of thymine. After photoexcitation at 267 nm, it undergoes $^1\pi\pi^*/^1n\pi^*$ internal conversion within (80 ± 30) fs. We do not find any evidence for competing relaxation channels proposed in the literature. Our study, furthermore, presents, for the first time, conclusive evidence for intersystem crossing from the $^1n\pi^*$ state to a $^3\pi\pi^*$ state within (3.5 ± 0.3) ps. This finding is an important contribution to the discussion of possible photodamage mechanisms in DNA.[23]

ASSOCIATED CONTENT

The following files are available free of charge.

Supporting Information including Supporting figures 1,2 and 3

AUTHOR INFORMATION

Corresponding Author

*thomas.wolf@stanford.edu, mguehr@uni-potsdam.de

Author Contributions

The manuscript was written through contributions of all authors. All authors have given approval to the final version of the manuscript.

Funding Sources

U.S. Department of Energy, Office of Science, Basic Energy Sciences, Chemical Sciences, Geosciences, and Biosciences Division

Office of Science Early Career Research Program through the Office of Basic Energy Sciences, U.S. Department of Energy under grant No. DE-SC0012376

Volkswagen foundation

German National Academy of Sciences Leopoldina (Grant No. LPDS2013-14)

ACKNOWLEDGMENT

This work was supported by the U.S. Department of Energy, Office of Science, Basic Energy Sciences, Chemical Sciences, Geosciences, and Biosciences Division. MG acknowledges funding via the Office of Science Early Career Research Program through the Office of Basic Energy Sciences, U.S. Department of Energy under grant No. DE-SC0012376. MG is now funded by a Lichtenberg Professorship from the Volkswagen foundation. TJAW thanks the German National Academy of Sciences Leopoldina for a fellowship (Grant No. LPDS2013-14).

REFERENCES

(1) Schreier, W. J.; Schrader, T. E.; Koller, F. O.; Gilch, P.; Crespo-Hernández, C. E.; Swaminathan, V. N.; Carell, T.; Zinth, W.; Kohler, B. Thymine Dimerization in DNA Is an Ultrafast Photoreaction. *Science* **2007**, *315* (5812), 625–629. https://doi.org/10.1126/science.1135428.

(2) Middleton, C. T.; de La Harpe, K.; Su, C.; Law, Y. K.; Crespo-Hernández, C. E.; Kohler, B. DNA Excited-State Dynamics: From Single Bases to the Double Helix. *Annual Review of Physical Chemistry* **2009**, *60* (1), 217–239. https://doi.org/10.1146/annurev.physchem.59.032607.093719.

(3) Crespo-Hernández, C. E.; Cohen, B.; Hare, P. M.; Kohler, B. Ultrafast Excited-State Dynamics in Nucleic Acids. *Chem. Rev.* **2004**, *104*, 1977.

(4) Improta, R.; Santoro, F.; Blancafort, L. Quantum Mechanical Studies on the Photophysics and the Photochemistry of Nucleic Acids and Nucleobases. *Chem. Rev.* **2016**, *116* (6), 3540–3593. https://doi.org/10.1021/acs.chemrev.5b00444.

(5) Keefer, D.; Thallmair, S.; Matsika, S.; de Vivie-Riedle, R. Controlling Photorelaxation in Uracil with Shaped Laser Pulses: A Theoretical Assessment. *J. Am. Chem. Soc.* **2017**. https://doi.org/10.1021/jacs.6b12033.

(6) Hudock, H. R.; Levine, B. G.; Thompson, A. L.; Satzger, H.; Townsend, D.; Gador, N.; Ullrich, S.; Stolow, A.; Martínez, T. J. Ab Initio Molecular Dynamics and Time-Resolved Photoelectron Spectroscopy of Electronically Excited Uracil and Thymine. *J. Phys. Chem. A* **2007**, *111* (34), 8500–8508. https://doi.org/10.1021/jp0723665.

(7) Mai, S.; Richter, M.; Marquetand, P.; González, L. The DNA Nucleobase Thymine in Motion – Intersystem Crossing Simulated with Surface Hopping. *Chemical Physics* **2017**, *482*, 9–15. https://doi.org/10.1016/j.chemphys.2016.10.003.

(8) Kang, H.; Lee, K. T.; Jung, B.; Ko, Y. J.; Kim, S. K. Intrinsic Lifetimes of the Excited State of DNA and RNA Bases. *J. Am. Chem. Soc.* **2002**, *124* (44), 12958–12959. https://doi.org/10.1021/ja027627x.

(9) He, Y.; Wu, C.; Kong, W. Decay Pathways of Thymine and Methyl-Substituted Uracil and Thymine in the Gas Phase. *The Journal of Physical Chemistry A* **2003**, *107* (26), 5145–5148. https://doi.org/10.1021/jp034733s.

(10) Ligare, M.; Siouri, F.; Bludsky, O.; Nachtigallova, D.; de Vries, M. S. Characterizing the Dark State in Thymine and Uracil by Double Resonant Spectroscopy and Quantum Computation. *Phys. Chem. Chem. Phys.* **2015**, *17* (37), 24336–24341. https://doi.org/10.1039/C5CP03516C.

(11) Yu, H.; Sanchez-Rodriguez, J. A.; Pollum, M.; Crespo-Hernández, C. E.; Mai, S.; Marquetand, P.; González, L.; Ullrich, S. Internal Conversion and Intersystem Crossing Pathways in UV Excited, Isolated Uracils and Their Implications in Prebiotic Chemistry. *Phys. Chem. Chem. Phys.* **2016**, *18* (30), 20168–20176. https://doi.org/10.1039/C6CP01790H.

(12) Barbatti, M.; Aquino, A. J. A.; Szymczak, J. J.; Nachtigallová, D.; Hobza, P.; Lischka, H. Relaxation Mechanisms of UV-Photoexcited DNA and RNA Nucleobases. *Proc. Natl. Acad. Sci. U.S.A.* **2010**, *107* (50), 21453–21458. https://doi.org/10.1073/pnas.1014982107.

(13) Yamazaki, S.; Taketsugu, T. Nonradiative Deactivation Mechanisms of Uracil, Thymine, and 5-Fluorouracil: A Comparative Ab Initio Study. *The Journal of Physical Chemistry A* **2012**, *116* (1), 491–503. https://doi.org/10.1021/jp206546g.

(14) Asturiol, D.; Lasorne, B.; Worth, G. A.; Robb, M. A.; Blancafort, L. Exploring the Sloped-to-Peaked S2/S1 Seam of Intersection of Thymine with Electronic Structure and Direct Quantum Dynamics Calculations. *Phys. Chem. Chem. Phys.* **2010**, *12* (19), 4949–4958. https://doi.org/10.1039/C001556C.

(15) Picconi, D.; Barone, V.; Lami, A.; Santoro, F.; Improta, R. The Interplay between $\Pi\pi^*/N\pi^*$ Excited States in Gas-Phase Thymine: A Quantum Dynamical Study. *ChemPhysChem* **2011**, *12* (10), 1957–1968. https://doi.org/10.1002/cphc.201001080.

(16) Nakayama, A.; Arai, G.; Yamazaki, S.; Taketsugu, T. Solvent Effects on the Ultrafast Nonradiative Deactivation Mechanisms of Thymine in Aqueous Solution: Excited-State QM/MM Molecular Dynamics Simulations. *The Journal of Chemical Physics* **2013**, *139* (21), 214304. https://doi.org/10.1063/1.4833563.

(17) Wolf, T. J. A.; Myhre, R. H.; Cryan, J. P.; Coriani, S.; Squibb, R. J.; Battistoni, A.; Berrah, N.; Bostedt, C.; Bucksbaum, P.; Coslovich, G.; et al. Probing Ultrafast $\Pi\pi^*$ / $N\pi^*$ Internal Conversion in Organic Chromophores via K-Edge Resonant Absorption. *Nature Communications* **2017**, *8* (1), 29. https://doi.org/10.1038/s41467-017-00069-7.

(18) Ullrich, S.; Schultz, T.; Zgierski, M. Z.; Stolow, A. Electronic Relaxation Dynamics in DNA and RNA Bases Studied by Time-Resolved Photoelectron Spectroscopy. *Phys. Chem. Chem. Phys.* **2004**, *6* (10), 2796–2801. https://doi.org/10.1039/B316324E.

(19) McFarland, B. K.; Farrell, J. P.; Miyabe, S.; Tarantelli, F.; Aguilar, A.; Berrah, N.; Bostedt, C.; Bozek, J. D.; Bucksbaum, P. H.; Castagna, J. C.; et al. Ultrafast X-Ray Auger Probing of Photoexcited Molecular Dynamics. *Nat. Commun.* **2014**, *5*, 4235.

(20) Canuel, C.; Mons, M.; Piuzzi, F.; Tardivel, B.; Dimicoli, I.; Elhanine, M. Excited States Dynamics of DNA and RNA Bases: Characterization of a Stepwise Deactivation Pathway in the Gas Phase. *J. Chem. Phys.* **2005**, *122* (7), 074316. https://doi.org/10.1063/1.1850469.

(21) Koch, M.; Wolf, T. J. A.; Gühr, M. Understanding the Modulation Mechanism in Resonance-Enhanced Multiphoton Probing of Molecular Dynamics. *Phys. Rev. A* **2015**, *91* (3), 031403(R). https://doi.org/10.1103/PhysRevA.91.031403.
(22) Horton, S. L.; Liu, Y.; Chakraborty, P.; Marquetand, P.; Rozgonyi, T.; Matsika, S.; Weinacht, T. Strong-Field- versus Weak-Field-Ionization Pump-Probe Spectroscopy. *Phys. Rev. A* **2018**, *98* (5), 053416. https://doi.org/10.1103/PhysRevA.98.053416.
(23) Kwok, W.-M.; Ma, C.; Phillips, D. L. A Doorway State Leads to Photostability or Triplet Photodamage in Thymine DNA. *J. Am. Chem. Soc.* **2008**, *130* (15), 5131–5139. https://doi.org/10.1021/ja077831q.
(24) Serrano-Pérez, J. J.; González-Luque, R.; Merchán, M.; Serrano-Andrés, L. On the Intrinsic Population of the Lowest Triplet State of Thymine. *J. Phys. Chem. B* **2007**, *111* (41), 11880–11883. https://doi.org/10.1021/jp0765446.
(25) Ernst, H. A.; Wolf, T. J. A.; Schalk, O.; Núria González-García; Boguslavskiy, A. E.; Stolow, A.; Olzmann, M.; Unterreiner, A.-N. Ultrafast Dynamics of O-Nitrophenol: An Experimental and Theoretical Study. *The Journal of Physical Chemistry A* **2015**, *119* (35), 9225–9235. https://doi.org/10.1021/acs.jpca.5b04900.
(26) Marian, C. M. Spin–Orbit Coupling and Intersystem Crossing in Molecules. *WIREs Comput Mol Sci* **2012**, *2* (2), 187–203. https://doi.org/10.1002/wcms.83.
(27) Schnappinger, T.; Kölle, P.; Marazzi, M.; Monari, A.; González, L.; Vivie-Riedle, R. de. Ab Initio Molecular Dynamics of Thiophene: The Interplay of Internal Conversion and Intersystem Crossing. *Phys. Chem. Chem. Phys.* **2017**, *19* (37), 25662–25670. https://doi.org/10.1039/C7CP05061E.
(28) Koch, M.; Wolf, T. J. A.; Grilj, J.; Sistrunk, E.; Gühr, M. Femtosecond Photoelectron and Photoion Spectrometer with Vacuum Ultraviolet Probe Pulses. *Journal of Electron Spectroscopy and Related Phenomena* **2014**, *197* (0), 22–29. http://dx.doi.org/10.1016/j.elspec.2014.08.006.
(29) Grilj, J.; Sistrunk, E.; Koch, M.; Gühr, M. A Beamline for Time-Resolved Extreme Ultraviolet and Soft X-Ray Spectroscopy. *J. Anal. Bioanal. Tech.* **2014**, No. 0, S12:005. https://doi.org/10.4172/2155-9872.S12-005.
(30) McFarland, B. K.; Berrah, N.; Bostedt, C.; Bozek, J.; Bucksbaum, P. H.; Castagna, J. C.; Coffee, R. N.; Cryan, J. P.; Fang, L.; Farrell, J. P.; et al. Experimental Strategies for Optical Pump - Soft x-Ray Probe Experiments at the LCLS. *Journal of Physics: Conference Series* **2014**, *488* (1), 012015.
(31) Shao, Y.; Gan, Z.; Epifanovsky, E.; Gilbert, A. T. B.; Wormit, M.; Kussmann, J.; Lange, A. W.; Behn, A.; Deng, J.; Feng, X.; et al. Advances in Molecular Quantum Chemistry Contained in the Q-Chem 4 Program Package. *Molecular Physics* **2015**, *113* (2), 184–215. https://doi.org/10.1080/00268976.2014.952696.
(32) Aidas, K.; Angeli, C.; Bak, K. L.; Bakken, V.; Bast, R.; Boman, L.; Christiansen, O.; Cimiraglia, R.; Coriani, S.; Dahle, P.; et al. The Dalton Quantum Chemistry Program System. *WIREs Comput Mol Sci* **2014**, *4* (3), 269–284. https://doi.org/10.1002/wcms.1172.
(33) Ufimtsev, I. S.; Martinez, T. J. Quantum Chemistry on Graphical Processing Units. 2. Direct Self-Consistent-Field Implementation. *J. Chem. Theory Comput.* **2009**, *5* (4), 1004–1015. https://doi.org/10.1021/ct800526s.
(34) Ufimtsev, I. S.; Martinez, T. J. Quantum Chemistry on Graphical Processing Units. 3. Analytical Energy Gradients, Geometry Optimization, and First Principles Molecular

Dynamics. *J. Chem. Theory Comput.* **2009**, *5* (10), 2619–2628. https://doi.org/10.1021/ct9003004.
(35) Ufimtsev, I. S.; Martínez, T. J. Quantum Chemistry on Graphical Processing Units. 1. Strategies for Two-Electron Integral Evaluation. *J. Chem. Theory Comput.* **2008**, *4* (2), 222–231. https://doi.org/10.1021/ct700268q.
(36) Luehr, N.; Ufimtsev, I. S.; Martínez, T. J. Dynamic Precision for Electron Repulsion Integral Evaluation on Graphical Processing Units (GPUs). *J. Chem. Theory Comput.* **2011**, *7* (4), 949–954. https://doi.org/10.1021/ct100701w.
(37) Becke, A. D. Density-Functional Thermochemistry. III. The Role of Exact Exchange. *J. Chem. Phys.* **1993**, *98* (7), 5648–5652. https://doi.org/10.1063/1.464913.
(38) Lee, C.; Yang, W.; Parr, R. G. Development of the Colle-Salvetti Correlation-Energy Formula into a Functional of the Electron Density. *Phys. Rev. B* **1988**, *37* (2), 785–789. https://doi.org/10.1103/PhysRevB.37.785.
(39) Vosko, S. H.; Wilk, L.; Nusair, M. Accurate Spin-Dependent Electron Liquid Correlation Energies for Local Spin Density Calculations: A Critical Analysis. *Can. J. Phys.* **1980**, *58* (8), 1200–1211. https://doi.org/10.1139/p80-159.
(40) Stephens, P. J.; Devlin, F. J.; Chabalowski, C. F.; Frisch, M. J. Ab Initio Calculation of Vibrational Absorption and Circular Dichroism Spectra Using Density Functional Force Fields. *J. Phys. Chem.* **1994**, *98* (45), 11623–11627. https://doi.org/10.1021/j100096a001.
(41) Hehre, W. J.; Ditchfield, R.; Pople, J. A. Self—Consistent Molecular Orbital Methods. XII. Further Extensions of Gaussian—Type Basis Sets for Use in Molecular Orbital Studies of Organic Molecules. *J. Chem. Phys.* **1972**, *56* (5), 2257–2261. https://doi.org/10.1063/1.1677527.
(42) Hariharan, P. C.; Pople, J. A. The Influence of Polarization Functions on Molecular Orbital Hydrogenation Energies. *Theoret. Chim. Acta* **1973**, *28* (3), 213–222. https://doi.org/10.1007/BF00533485.
(43) Isborn, C. M.; Luehr, N.; Ufimtsev, I. S.; Martínez, T. J. Excited-State Electronic Structure with Configuration Interaction Singles and Tamm–Dancoff Time-Dependent Density Functional Theory on Graphical Processing Units. *J. Chem. Theory Comput.* **2011**, *7* (6), 1814–1823. https://doi.org/10.1021/ct200030k.
(44) Trofimov, A. B.; Schirmer, J.; Kobychev, V. B.; Potts, A. W.; Holland, D. M. P.; Karlsson, L. Photoelectron Spectra of the Nucleobases Cytosine, Thymine and Adenine. *Journal of Physics B: Atomic, Molecular and Optical Physics* **2006**, *39* (2), 305.
(45) Schalk, O.; Boguslavskiy, A. E.; Stolow, A.; Schuurman, M. S. Through-Bond Interactions and the Localization of Excited-State Dynamics. *J. Am. Chem. Soc.* **2011**, *133* (41), 16451–16458. https://doi.org/10.1021/ja1114002.
(46) Wolf, T. J. A.; Kuhlman, T. S.; Schalk, O.; Martinez, T. J.; Moller, K. B.; Stolow, A.; Unterreiner, A.-N. Hexamethylcyclopentadiene: Time-Resolved Photoelectron Spectroscopy and Ab Initio Multiple Spawning Simulations. *Phys. Chem. Chem. Phys.* **2014**, *16*, 11770–11779. https://doi.org/10.1039/C4CP00977K.
(47) Blanchet, V.; Zgierski, M. Z.; Stolow, A. Electronic Continua in Time-Resolved Photoelectron Spectroscopy. I. Complementary Ionization Correlations. *J. Chem. Phys.* **2001**, *114* (3), 1194–1205. https://doi.org/10.1063/1.1331636.
(48) Blanchet, V.; Zgierski, M. Z.; Seideman, T.; Stolow, A. Discerning Vibronic Molecular Dynamics Using Time-Resolved Photoelectron Spectroscopy. *Nature* **1999**, *401* (6748), 52–54.

(49) Asturiol, D.; Lasorne, B.; Robb, M. A.; Blancafort, L. Photophysics of the Ππ* and Nπ* States of Thymine: MS-CASPT2 Minimum-Energy Paths and CASSCF on-the-Fly Dynamics. *J. Phys. Chem. A* **2009**, *113* (38), 10211–10218. https://doi.org/10.1021/jp905303g.
(50) Szymczak, J. J.; Barbatti, M.; Soo Hoo, J. T.; Adkins, J. A.; Windus, T. L.; Nachtigallová, D.; Lischka, H. Photodynamics Simulations of Thymine: Relaxation into the First Excited Singlet State. *J. Phys. Chem. A* **2009**, *113* (45), 12686–12693. https://doi.org/10.1021/jp905085x.
(51) Mori, T.; Glover, W. J.; Schuurman, M. S.; Martínez, T. J. Role of Rydberg States in the Photochemical Dynamics of Ethylene. *J. Phys. Chem. A* **2012**, *116* (11), 2808–2818. https://doi.org/10.1021/jp2097185.
(52) Schneider, M.; Maksimenka, R.; Buback, F. J.; Kitsopoulos, T.; Lago, L. R.; Fischer, I. Photodissociation of Thymine. *Phys. Chem. Chem. Phys.* **2006**, *8* (25), 3017–3021. https://doi.org/10.1039/B518443F.